Bull. Mater. Sci., Vol. 37, No. 3, May 2014, pp. 473–480. © Indian Academy of Sciences.

A.c. conductivity and dielectric study of $LiNiPO_4$ synthesized by solid-state method

M BEN BECHIR, A BEN RHAIEM* and K GUIDARA

University of Sfax, Faculty of Sciences, Condensed Matter Laboratory, B. P. 1171, 3000 Sfax, Tunisia

MS received 21 February 2013; revised 12 May 2013

Abstract. **$LiNiPO_4$ compound was prepared by the conventional solid-state reaction. The sample was characterized by X-ray powder diffraction, infrared, Raman analysis spectroscopy and electrical impedance spectroscopy. The compound crystallizes in the orthorhombic system, space group *Pnma* with $a = 10{\cdot}0252(7)$ Å, $b = 5{\cdot}8569(5)$ Å and $c = 4{\cdot}6758(4)$ Å. Vibrational analysis was used to identify the presence of PO_4^{3-} group in this compound. The complex impedance has been measured in the temperature and frequency ranges 654–716 K and 242 Hz–5 MHz, respectively. The Z' and Z'' vs frequency plots are well-fitted to an equivalent circuit consisting of series of combination of grains and grain boundary elements. Dielectric data were analysed using complex electrical modulus M^* for the sample at various temperatures. The modulus plots are characterized by the presence of two peaks thermally activated. The frequency dependence of the conductivity is interpreted in terms of equation: $\sigma_{a.c.}(\omega) = [\sigma_g/(1 + \tau^2\omega^2) + (\sigma_\infty\tau^2\omega^2/1 + \tau^2\omega^2) + A\omega^n]$. The near values of activation energies obtained from the analysis of M'', conductivity data and equivalent circuit confirms that the transport is through ion hopping mechanism dominated by the motion of Li^+ in the structure of the investigated material.**

Keywords. **$LiNiPO_4$; complex impedance; a.c. conductivity; dielectric modulus.**

1. Introduction

For years, lithium orthophosphates $LiMPO_4$ (M = Fe, Mn, Co, Ni, etc.) have been a lot of interest as cathodes for use in Li-ion batteries (Okada *et al* 2001; Yamada *et al* 2003). They have a stable structure on the charging/discharging, thermal stability (Wang *et al* 2004; Molenda 2005; Wang *et al* 2005). However, they have a low capacity because of the weakness of the electronic and ionic conductivities. Lithium orthophosphates $LiMPO_4$ (M = Mn, Co, Ni) adopt an olivine-related structure, in the structure olivine octahedral sites are occupied by two types of cations (M^{2+} and Li^+), which allows us to establish an order between these two cations. The structure is formed by NiO_6 octahedral and PO_4 tetrahedral linked by edges and vertices. This three-dimensional network delimited in tunnels in the directions [010] and [001], in which octahedrally coordinated Li^+ are inserted (Newnham and Redham 1965; Abrahams and Easson 1993).

The orthorhombic structure of $LiNiPO_4$ is described in the space group *Pnma*. All the ions are located in specific positions 4*c* on the plane mirror, except the lithium which is located in position 4*a* and one of the three atoms of oxygen, which is in position 8*d*. An octahedron NiO_6 is linked to four other octahedral NiO_6 by sharing of summits, which limit the electronic conductivity, but also to five tetrahedrons PO_4 including one by a ridge. The layers of octahedral form and of the checkerboards are in the plane *bc*. These layers are connected by the tetrahedrons PO_4, the latter *s* play a role of pillars in the structure. The polyhedra of lithium LiO_6 form of channels according to the *b*-axis by sharing the edges in the plane *bc* (Abrahams and Easson 1993) (figure 1).

As continuity and in order to study effect of the substitution of M in $LiMPO_4$ compound by a smaller cation radius, we have synthesized $LiNiPO_4$ compound. In this paper, we analyse IR and Raman spectroscopies, the dielectric properties and the conduction behaviour of the lithium orthophosphate $LiNiPO_4$.

2. Experimental

2.1 *Synthesis*

Synthesis of polycrystalline powder of $LiNiPO_4$ was carried out by conventional solid-state reaction techniques. Stoichiometric quantities of Li_2CO_3, $(NH_4)_2HPO_4$, and NiO were well grounded, mixed, and progressively heated first to 393 K to expel NH_3, H_2O and CO_2, then the powders were pressed into pellets of 8 mm diameter and sintered at 773 K for 48 h.

*Author for correspondence (abdallahrhaiem@yahoo.fr)

2.2 *Apparatus*

At room temperature, the sample was characterized by X-ray powder pattern using a Philips PW 1710 diffractometer operating with copper radiation $\lambda_{K_\alpha} = 1{\cdot}5418$ Å. Unit cell parameters of the synthesized compound have been refined by the least-square method from the powder data. Infrared absorption spectrum was recorded at room temperature between 1200 and 400 cm^{-1} with a BX FTIR spectrometer (Perkin–Elmer). Raman spectrum was recorded between 1200 and 50 cm^{-1} with a Kaiser Hololab 5000R Raman spectrometer at room temperature. Before electrical measurements, the polycrystalline $LiNiPO_4$ sample was pressed into pellets of 8 mm diameter and 1·5 mm thickness using $3t/cm^2$ uniaxial pressure. A.c. impedance data were measured in the frequency range from 242 Hz to 5 MHz with TEGAM 3550 ALF automatic bridge monitored by a microcomputer between 654 and 716 K.

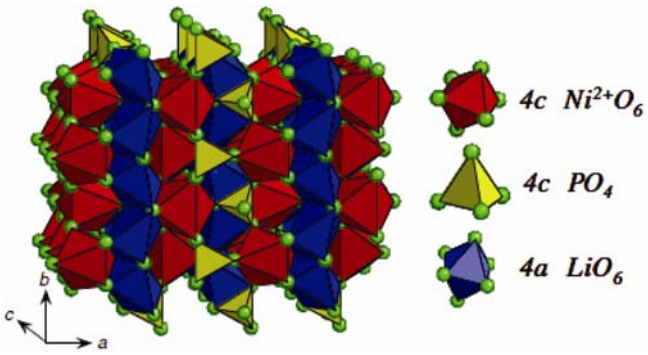

Figure 1. Schematic drawing of crystal structure of $LiNiPO_4$.

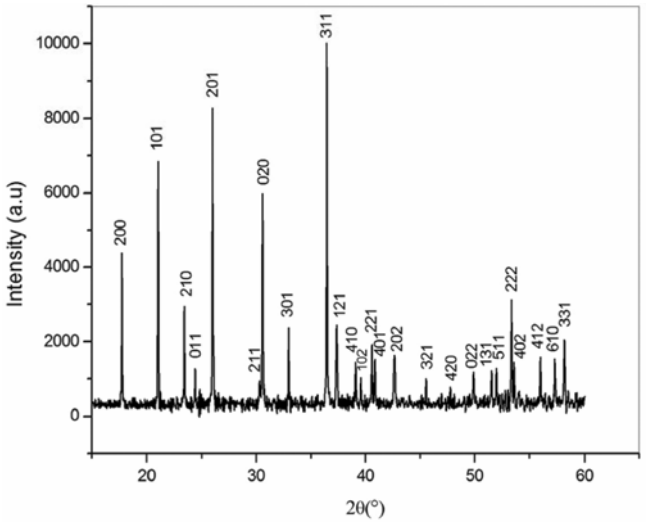

Figure 2. X-ray diffractogram of $LiNiPO_4$ in 2θ range of 5 to 60°.

2.3 *X-ray powder analysis*

X-ray powder diffractogram (figure 2) reveals that the synthesized compound crystallizes in the orthorhombic system with the space group *Pnma* and the refined unit cell parameters are: $a = 10{\cdot}0252(7)$ Å, $b = 5{\cdot}8569(5)$ Å, $c = 4{\cdot}6758(4)$ Å and $V = 274{\cdot}546$ $Å^3$, which are in good agreement with the literature values (Warda *et al* 1997).

In $LiMPO_4$ series (M = Ca, Mn, Co, Fe and Ni), we can correlate the volume per unit molecular formula and M–O bond distances of these materials with the divalent cation radii (table 1). In figure 3, we plot the variation of the volume per unit molecular formula and M–O bond distances with the mean ionic radii of the divalent cation. We can assure that the volume/Z and M–O bond distances exhibit a linear dependence with the mean ionic radii of the divalent cation.

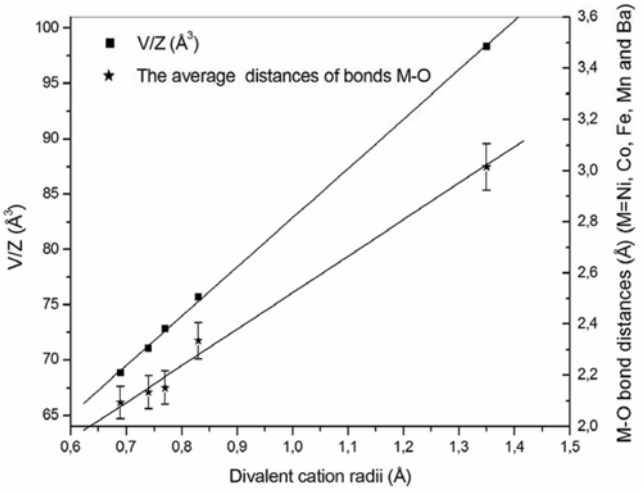

Figure 3. Variation of unit cell volume/Z and M–O bond distances as a function of mean ionic radii of Li orthophosphates.

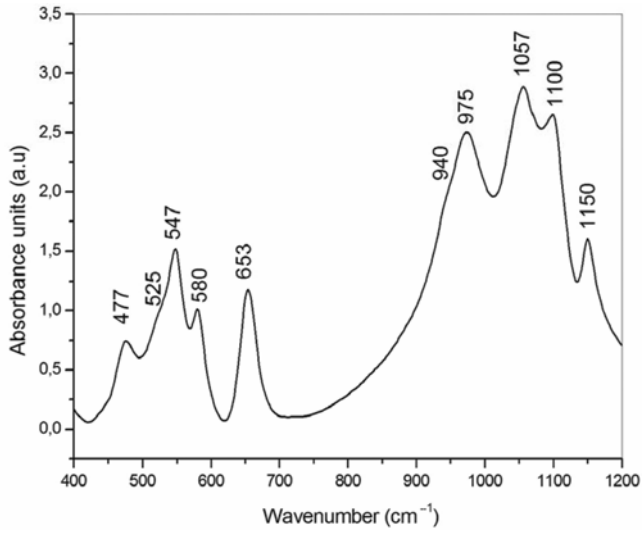

Figure 4. IR spectrum of $LiNiPO_4$ at room temperature.

Table 1. Unit cell volume, divalent cation radii and M–O bond distances of $LiMPO_4$ (M = Ni, Co, Fe, Mn, Ba) compounds.

Compounds	Z	Unit cell volume (V) ± (0·3 Å^3)	V/Z (Å^3)	Divalent cation radii (Å)	M–O bond distances (M = Ni, Co, Fe, Mn and Ba)
$LiNiPO_4$	4	275·3	68·82	0·69	2·045–2·144 Å
$LiCoPO_4$	4	284·2	71·05	0·74	2·046–2·223 Å
$LiFePO_4$	4	290·7	72·8	0·77	2·058–2·246 Å
$LiMnPO_4$	4	302	75·7	0·83	2·232–2·438 Å
$LiBaPO_4$	4	391·577	98·35	1·35	2·773–3·258 Å

Table 2. Vibrational spectra data (cm^{-1}) and band assignments in $LiNiPO_4$.

Infrared wavenumber (cm^{-1})	Raman wavenumber (cm^{-1})	Assignment
	116	External modes
	165	
	170	
	233	
	252	
	280	
	300	
	320	
477	460	ν (Li–O)
525		ν (Ni–O)
547		ν_2 $(PO4)^{3-}$
580	575	ν_2 $(PO4)^{3-}$
	590	ν_4 $(PO4)^{3-}$
	597	ν_4 $(PO4)^{3-}$
653	637	ν_4 $(PO4)^{3-}$
940	946	ν_1 $(PO4)^{3-}$
975	1009	ν_3 $(PO4)^{3-}$
1057		ν_3 $(PO4)^{3-}$
1100	1070	ν_3 $(PO4)^{3-}$
1150	1085	ν_3 $(PO4)^{3-}$

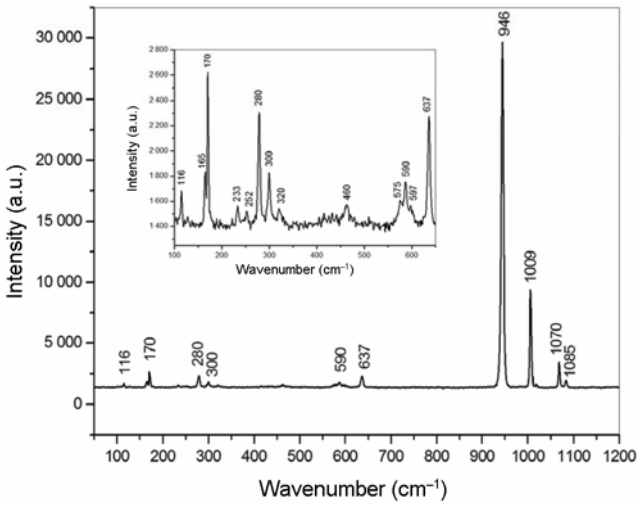

Figure 5. Raman spectrum of $LiNiPO_4$ at room temperature.

2.4 *IR and Raman spectroscopy*

The infrared and Raman spectra of the studied compound are shown successively in figures 4 and 5, whereas, their bands assignments are summarized in table 2. All of the bands observed between 1185 and 940 cm^{-1} are related to stretching mode of the tetrahedral $(PO_4)^{3-}$, ν_1 and ν_3 involve the symmetric and antisymmetric stretching mode of P–O bonds. All of the bonds observed between 653 and 547 cm^{-1} are related to bending mode of the tetrahedral $(PO_4)^{3-}$, ν_2 and ν_4 involve the symmetric and antisymmetric bending modes of O–P–O bonds (Nakamoto 1978). The peak at 525 cm^{-1} is essentially due to the translation modes of the Ni–O bonds. The bonds at 460 and 477 cm^{-1} are attributed to vibrations of Li–O bonds (Walrafen *et al* 1962; Julien 2000). The bonds observed below 400 cm^{-1} are related to external modes.

2.5 *Impedance analysis*

The impedance diagrams of $LiNiPO_4$ compound taken in the temperature range 654–716 K are shown in figure 6. There are two semicircles in each impedance spectrum. The low frequency semicircle is due to the grain boundary and the higher depicts the bulk (grain) effect (Macdonald 1987).

The impedance components were fitted to an equivalent circuit realized by two elements. The first consists of parallel combination of resistance (R_1) and constant phase elements (CPE_1) whereas the second consists of parallel

Table 3. Extract parameters for circuit elements.

T(K)	R_1 (10^5 Ω)	Q_1 (pF)	α_1	R_2 (10^6 Ω)	Q_2 (nF)	α_2
654	5·228	56	0·84	6·989	0·417	0·91
662	4·299	61	0·85	6·134	0·530	0·89
670	2·128	64	0·93	5·444	0·652	0·86
679	1·605	70·3	0·9	4·368	0·670	0·87
689	1·53	75	0·94	3·485	0·668	0·87
702	1·28	119·5	0·92	2·8	0·719	0·87
716	1·0016	164	0·95	2·336	0·817	0·86

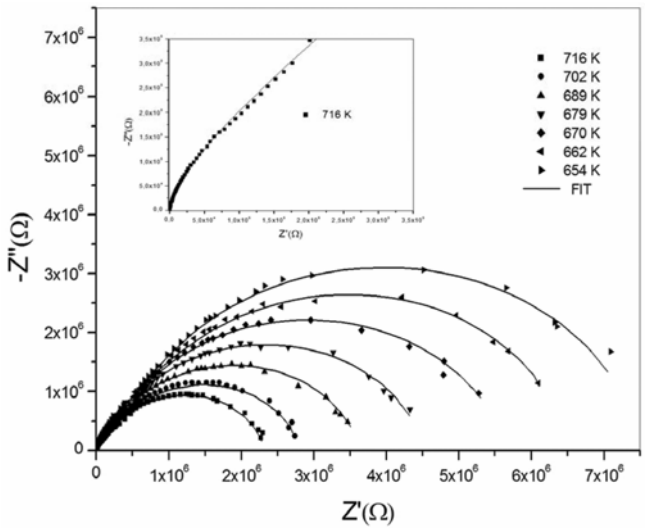

Figure 6. Nyquist plots (Z'' vs Z') of impedance data of $LiNiPO_4$ at different temperatures; inset one is a typical plot at 716 K. Solid line is simulated spectra.

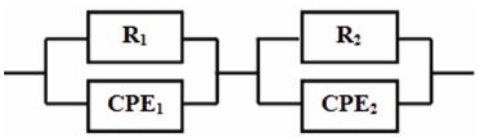

Figure 7. Equivalent circuit for $LiNiPO_4$.

combination of resistance (R_2) and constant phase elements (CPE_2) (figure 7).

The impedance of capacity of the fractal interface CPE is:

$$Z_{CPE} = 1/(Q(j\omega)^{\alpha}),$$

where Q indicates the value of capacitance of CPE element and α is the fractal exponent. The real and imaginary components of the whole impedance of this circuit were calculated according to the following expressions:

$$z' = \frac{R_1 + R_1^2 Q_1 \omega^{\alpha_1} \cos(\alpha_1\pi/2)}{(1 + R_1 Q_1 \omega^{\alpha_1} \cos(\alpha_1\pi/2))^2 + (R_1 Q_1 \omega^{\alpha_1} \sin(\alpha_1\pi/2))^2}$$

$$+ \frac{R_2 + R_2^2 Q_2 \omega^{\alpha_2} \cos(\alpha_2\pi/2)}{(1 + R_2 Q_2 \omega^{\alpha_2} \cos(\alpha_2\pi/2))^2 + (R_2 Q_2 \omega^{\alpha_2} \sin(\alpha_2\pi/2))^2},$$

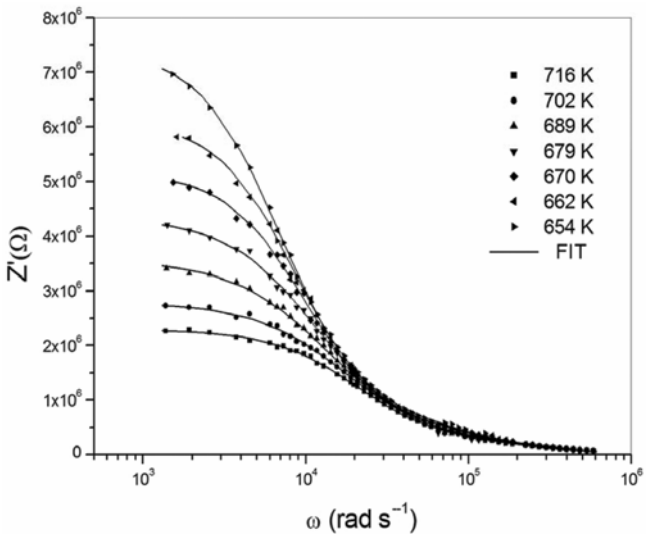

Figure 8. Variation of real part of impedance as a function of angular frequency at several temperatures. Solid line is a fit of experimental data.

$$-z'' = \frac{R_1^2 Q_1 \omega^{\alpha_1} \sin(\alpha_1\pi/2)}{(1 + R_1 Q_1 \omega^{\alpha_1} \cos(\alpha_1\pi/2))^2 + (R_1 Q_1 \omega^{\alpha_1} \sin(\alpha_1\pi/2))^2}$$

$$+ \frac{R_2^2 Q_2 \omega^{\alpha_2} \sin(\alpha_2\pi/2)}{(1 + R_2 Q_2 \omega^{\alpha_2} \cos(\alpha_2\pi/2))^2 + (R_2 Q_2 \omega^{\alpha_2} \sin(\alpha_2\pi/2))^2}.$$

Figures 8 and 9 show Z' and $-Z''$ vs frequency at different temperatures, respectively together with fits to the equivalent circuit of $LiNiPO_4$. A good agreement between calculated lines with experimental data indicates that the suggested equivalent circuit describes the pellet–electrolyte interface reasonably well. Fitted values of different parameters for the circuit elements are listed in table 3. The values of the capacity Q_1 is about of the picofarad which implies that the semicircles observed at high frequency represent the bulk response of the system. The values of the capacity Q_2 is about of the nanofarad which implies that the semicircles observed at low frequencies represent the grain boundary response of the system. The values of α_1 and α_2 are very close to 1, which confirm the weak interaction between localized sites in the material.

The temperature dependence of the grain boundary conductivity (σ_{gb}) and grain electrical conductivity (σ_g) are represented in figure 10. An Arrhenius type beha-

viour, $\sigma_{g,gb}T = \sigma_{g0,gb0}\exp(-E_{g,gb}/kT)$ is shown. σ_{gb0} and σ_{g0} are the pre-exponential factor, E_{gb} and E_g are the conductivity activation energy.

Both σ_g and σ_{gb} increase with increasing temperature, showing that the electrical conduction in the material is a thermally activated process. The bulk (E_g) and the grain boundary bulk (E_{gb}) conductivity activation energy were 0·68 and 0·67 eV, respectively. We notice that the bulk and the grain boundary activation energy values are almost equal. This indicates that the grain boundary conduction and grain conduction increase at a resembling rate with increase in temperature.

2.6 *Modulus analysis*

The electric modulus formula was created by Macedo *et al* (1972) and Moynihan *et al* (1973), which is a good method to study the polarization effect. The electric modulus can be calculated by using the following equation:

$$M^* = j\omega C_0 Z^* = j\omega C_0 (Z' - jZ''),$$

where $M' = \omega C_0 Z''$ and $M'' = \omega C_0 Z'$.

Figure 11 shows variation of imaginary part of electric modulus as an angular frequency function at several temperatures.

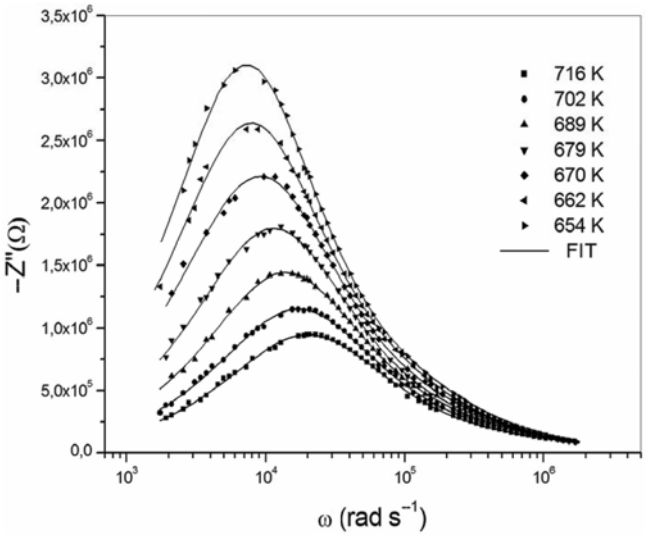

Figure 9. Variation of imaginary part of impedance as a function of angular frequency at several temperatures. Solid line is a fit of experimental data.

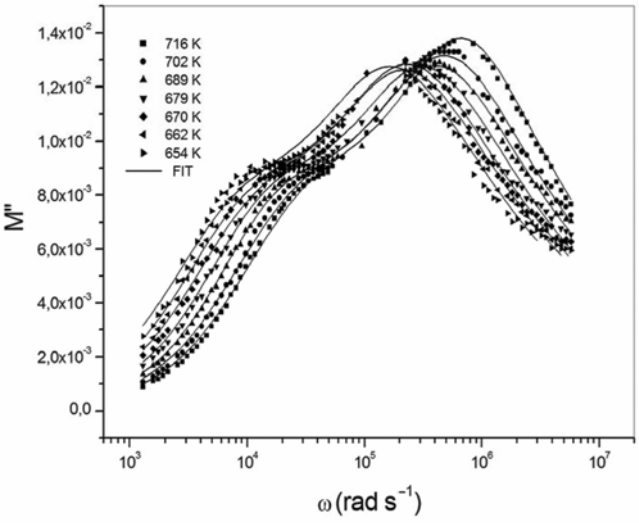

Figure 11. Angular frequency dependence of imaginary part of electric modulus at different temperatures. Solid line is a fit of experimental data.

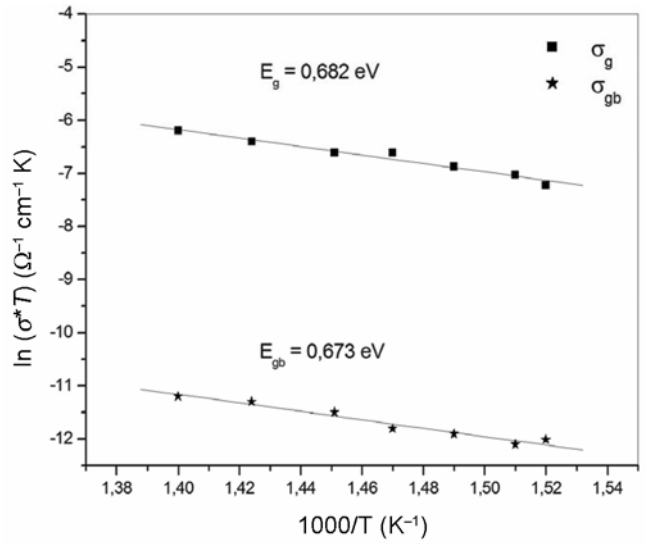

Figure 10. Variation of σ_g and σ_{gb} as a function of temperature.

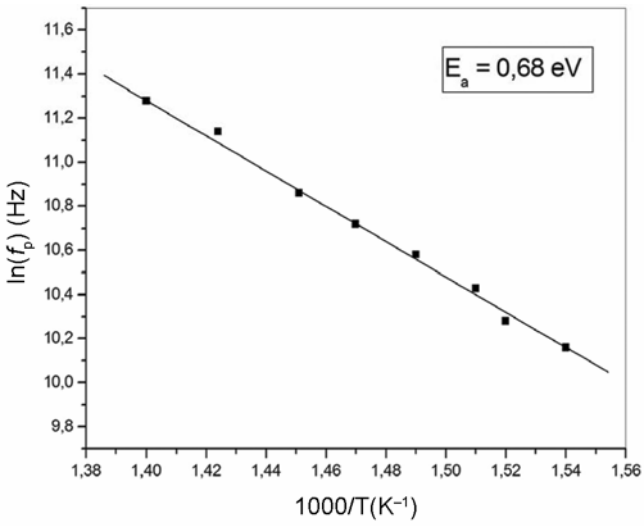

Figure 12. Temperature dependence of bulk relaxation frequency f_p obtained from frequency dependent plots of M'' for $LiNiPO_4$.

Double peaks are observed in the patterns. The most intense peaks are associated with the grain effect (these peaks shift toward higher angular frequencies with increasing temperature) the others are associated with the effects of grain boundaries.

The general method to study nature of the dielectric relaxation in the compound is to fit the measured data by Kohlrausch–Williams–Watts (KWW) decay function

$$\phi(t) = \exp\left[-\left(\frac{t}{\tau_m}\right)^{\beta}\right] \quad (0 \le \beta \le 1),$$

where τ_m is the characteristic relaxation time and β characterizes the degree of non-Debye behaviour.

$\phi(t)$ is associated to the modulus in the frequency domain by the equation (Kanchan *et al* 2009):

$$M^*(\omega) = M_\infty\left[1 - \int_0^\infty \exp(-j\omega t)\left(-\frac{d\phi(t)}{dt}\right)\right]dt.$$

Bergman (2000) was offered an approximate KWW function which permits a more simple analysis of the imaginary part of the complex modulus

$$M''(\omega) = \frac{M''_{max}}{\left((1-\beta)+\left(\frac{\beta}{1+\beta}\right)\right)\left[\beta\left(\frac{\omega_{max}}{\omega}\right)+\left(\frac{\omega}{\omega_{max}}\right)^{\beta}\right]},$$

where M''_{max} and ω_{max} are the peak maximum and peak angular frequency of the imaginary part of the modulus, respectively.

The experimental data have been fitted to the double Bergman's equation (we take into account the grain boundary effects). Good agreement was obtained between the experimental and calculated data (figure 10).

The β parameter value acquired for high-frequency peak was found to be between 0·39 and 0·52. For the peak at low frequency, the parameter β is found to be between 0·23 and 0·27.

The maximum in the well-defined peak of M'' curves corresponds to the bulk relaxation frequency f_p such as:

$$f_p = 1°/(2\pi\tau_c).$$

The variation of the frequency f_p with temperature follows the Arrhenius relation (figure 12):

$$f_p = f_0 \exp(-E_a/kT),$$

where f_0 is the frequency at infinite temperature and E_a is the activation energy. The activation energy extracted from the slope of the plot is 0·68 eV.

2.7 *Conductivity*

The angular frequency variation of a.c. conductivity at several temperatures for $LiNiPO_4$ compound is shown in figure 13. The conductivity of the sample has dispersed at all frequencies.

The phenomenon of the conductivity dispersion is analysed by the equation (Dussauze 2005):

$$\sigma_{a.c.}(\omega) = \frac{\sigma_g}{1+\tau^2\omega^2} + \frac{\sigma_\infty\tau^2\omega^2}{1+\tau^2\omega^2} + A\omega^n,$$

where σ_s is the conductivity at low frequencies, σ_∞ is an estimate of conductivity at high frequencies, $\omega = 2\pi f$ is the angular frequency, τ represents the characteristic relaxation time, A is a pre-exponential constant and n is the power law exponent, where $0 < n < 1$. n represents the degree of interaction between mobile ions with the environments surrounding them and A determines the strength of polarizability.

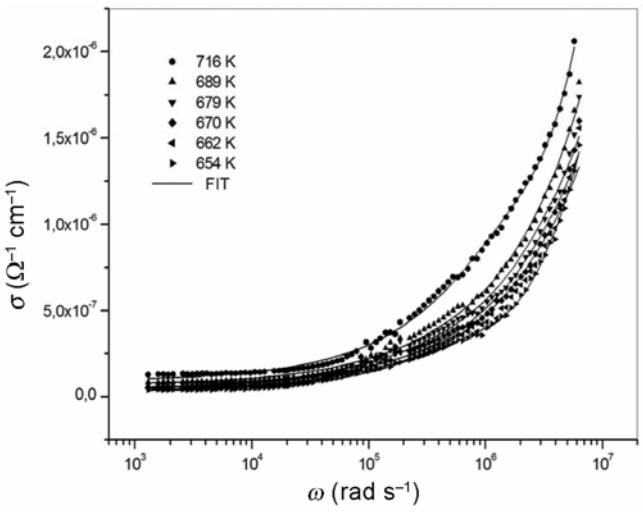

Figure 13. Frequency dependence of a.c. conductivity at various temperatures.

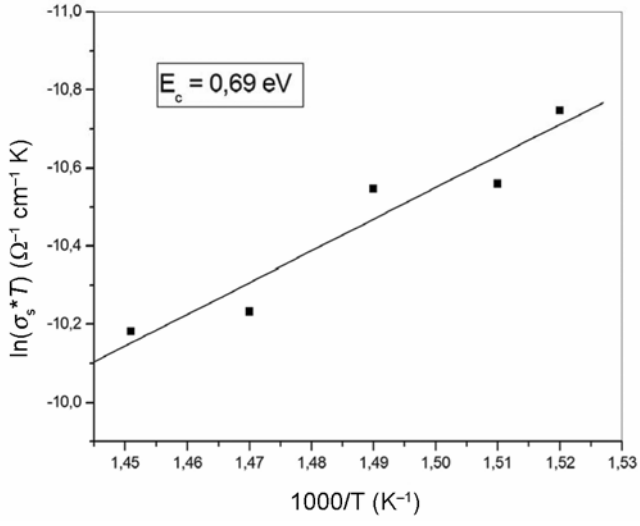

Figure 14. Dependence of $\ln(\sigma_s{*}T)$ on temperature for $LiNiPO_4$.

Table 4. Unit cell volume, divalent cation radii and electrical properties of $LiMPO_4$ (M = Ni, Ba) compounds.

Compound	Z	Unit cell volume (V) ± (0·3 Å^3)	V/Z (Å^3)	Divalent cation radii (Å)	Activation energy (eV)	β	$\sigma_{716\ K}$ (Ω^{-1} cm^{-1})
$LiNiPO_4$	4	275·3	68·82	0·69	0·69	0·39–0·52	$1{\cdot}15 \times 10^{-7}$
$LiBaPO_4$	4	391·577	98·35	1·35	1·20	0·61	$1{\cdot}9 \times 10^{-8}$
$LiCaPO_4$	6	488·02	81·33	0·99	0·9	0·66–0·74	$2{\cdot}21 \times 10^{-8}$

The values of n varied in the range (0·543–0·697) and the values of the parameter τ are similar to those determined by modulus study. The variation of d.c. conductivity (σ_g) are plotted in Arrhenius format as $\ln(T\sigma_g)$ vs 1000/T (figure 14), and all show Arrhenius-type behaviour described by:

$$T_g = \sigma_0 \exp(-E_c/kT),$$

where σ_g is the pre-exponential factor and E_c is the activation energy. The activation energy extracted from the slope of the plot is 0·69 eV. The near value of activation energies obtained from the analyses of modulus and conductivity data confirms that the conductivity is probably caused by the hopping of Li^+ in the tunnels [010] and [100] (Ben-Rhaiem *et al* 2009, 2010; Chouaib *et al* 2011).

The low frequency limit σ of the bulk a.c. $\sigma_{d.c.}$ conductivity determined by the impedance spectroscopy is governed mainly by the hopping rate of free charge carriers and the charge carrier concentration $N(T)$:

$$\sigma_{d.c.} = e^2 N(T) \gamma a_h^2 (\nu_0/kT) \exp(S_\mu/k) \exp(-E_c/kT),$$

(Hong 1976),

where a_h is the hopping distance; γ is a geometrical factor equal to 1/6 for isotropic media; ν_0 is an attempt frequency to overcome the potential barrier; S_μ is the migration entropy; E_μ is the migration energy; the other parameters having their conventional meaning (Hong 1976; Almond and West 1987; Uvarov *et al* 1994).

The electrical properties of $LiNiPO_4$ can be compared with those relative to $LiBaPO_4$ (Louati and Guidara 2012) and $LiCaPO_4$ (Louati and Guidara 2011) (table 4). The best properties obtained for $LiNiPO_4$ can be attributed to the following:

- A smaller E_c activation energy from $LiNiPO_4$ than $LiBaPO_4$ and $LiCaPO_4$ (table 2). The difference in the activation energy is accredited to a shrinking lattice effect. It is suggested that, for smaller lattice, the decreasing size of the cavities, in which the lithium ions reside, brings these cations closer to M^{2+} ions, consequently, the increasing repulsion between Li^+ and M^{2+} reduces the strength of Li–O bonds resulting in lower activation energy and higher conductivity (Subramanian *et al* 1986).
- A larger migration entropy term resulting from a more important disorder in Ni-metal than for Ba- and Ca-metals. The increase of entropy term is confirmed by the decrease of β parameter (table 2).

3. Conclusions

In summary, in this work, we have synthesized $LiNiPO_4$ compound by the classic ceramic method. X-ray diffraction analysis shows that the compound is orthorhombic with *Pnma* space group. The impedance plots show two semicircles, which confirms the presence of two relaxation processes in the sample associated with the grain and grain boundary. The dielectric data have been analysed in modulus formalism with a distribution of relaxation times using KWW stretched exponential function. The presence of two relaxation peaks thermally activated in the modulus loss spectra confirmed the grain and grain boundary contribution to electrical response in the material. The conductivity of $LiNiPO_4$ has been analysed as a function of temperature and frequency. The values of activation energies obtained from the analysis of equivalent circuit, dielectric and conductivity data are near and confirms that the electrical conduction in lithium orthophosphate $LiNiPO_4$ sample is presumably caused by the hopping of Li^+ between sites along the [010] and [100] directions. The electrical properties have been discussed as a function of variations in the activation energy and β parameter.

References

Abrahams C M I and Easson K S 1993 *Acta Crystallogr. Sect.* **C49** 925

Almond D P and West A R 1987 *Solid State Ionics* **23** 27

Ben Rhaiem A, Hlel F, Guidara K and Gargouri M 2009 *J. Alloys Compd.* **485** 718

Ben Rhaiem A, Chouaib S and Guidara K 2010 *Solid State Ionics* **16** 455

Bergman R 2000 *J. Appl. Phys.* **88** 1356

Chouaib S, Ben Rhaiem A and Guidara K 2011 *Bull. Mater. Sci.* **34** 915

Dussauze M 2005 Génération de second harmonique dans des verres borophosphate de sodium et niobium par polarisation thermique, Université bordeaux I, Thèse

Hong H Y P 1976 *Mater. Res. Bull.* **11** 173

Julien C 2000 *Ionics* **6** 30

Kanchan D K, Pant M and Gondaliya N 2009 *Mater. Chem. Phys.* **115** 98

Louati B and Guidara K 2011 *Solid State Ionics* **17** 633

Louati B and Guidara K 2012 *Mater. Sci. Eng.* **B177** 771

Macdonald J R (ed.) 1987 *Impedance spectroscopy: emphasizing solid materials and systems* (New York: Wiley)

Macedo P B, Moynihan C T and Bose R 1972 *Phys. Chem. Glasses* **13** 171

Molenda J 2005 *Solid State Ionics* **176** 1687

Moynihan C T, Boesch L P and Laberge L 1973 *Phys. Chem. Glasses* **14** 122

Nakamoto K 1978 *Infrared and Raman spectra of inorganic and coordination compounds* (New York: John Wiley & Sons) (3rd ed.)

Newnham R E and Redham M J 1965 *J. Am. Ceram. Soc.* **48** 547

Okada S, Sawa S, Egashira M, Yamaki J, Tabuchi M, Kageyama H, Konishi T and Yoshinof A 2001 *J. Power Sources* **430** 97

Subramanian M A, Subramanian R and Clearfield A 1986 *Solid State Ionics* **18** 562

Uvarov N F, Hairetdinov E F, Reau J M, Bobe J M, Senegas J and Poulain M 1994 *Solid State Ionics* **74** 195

Walrafen G E, Irish D E and Young F 1962 *J. Chem. Phys.* **37** 662

Wang D, Li H, Shi S, Huang X and Chen L 2005 *Electrochimica Acta* **50** 2955

Wang G X, Bewaly S L, Konstantino K, Liu H K, Dou S X and Ahn J-H 2004 *Electrochimica Acta* **50** 443

Warda S A, Lee S-L and Krist Z 1997 *New Cryst. St.* **212** 319

Yamada A, Hosoya M, Chung S-C, Kudo Y, Hinokuma K, Liu K-Y and Nishi Y 2003 *J. Power Sources* **232** 119